Journal of Colloid and Interface Science 679 (2025) 939–946

Contents lists available at ScienceDirect

Journal of Colloid And Interface Science

journal homepage: www.elsevier.com/locate/jcis

Regular Article

Deposit of Red Blood Cells at low concentrations in evaporating droplets is dominated by a central edge growth

Vahideh Sardari [a,b], Mahsa Mohammadian [b], Shima Asfia [b], Felix Maurer [b], Diana Örüm [b], Ralf Seemann [b], Thomas John [b], Lars Kaestner [b,c], Christian Wagner [b,d], Maniya Maleki [a], Alexis Darras [b,*]

[a] Department of Physics, Institute for Advanced Studies in Basic Sciences (IASBS), Zanjan, 45137-66731, Iran
[b] Department of Experimental Physics & Center for Biophysics, Saarland University, Saarbruecken, D-66123, Germany
[c] Department of Theoretical Medicine and Biosciences, Saarland University, Homburg, D-66421, Germany
[d] Physics and Materials Science Research Unit, University of Luxembourg, Luxembourg, L-4365, Luxembourg

GRAPHICAL ABSTRACT

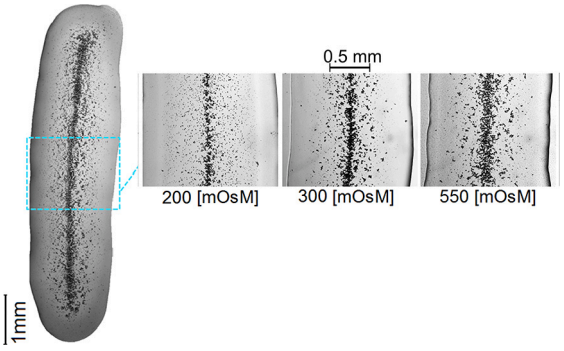

ABSTRACT

Evaporation of blood droplets and diluted blood samples is a topic of intensive research, as it is considered a potential low-cost diagnostic tool. So far, samples with a volume fraction down to a few percent of red blood cells have been studied, and these were reportedly dominated by a “coffee-ring” deposit. In this study, samples with lower volume fractions were used to investigate the growth of the evaporative deposit from sessile droplets in more detail. We observed that blood samples and salt solutions with less than 1% volume fraction of red blood cells are dominated by a central deposit. We characterized the growth process of this central deposit by evaporating elongated drops and determined that it is consistent with the Kardar-Parisi-Zhang process in the presence of quenched disorder. Our results showed a sensitivity of the deposit size to fibrinogen concentration and the shape of red blood cells, suggesting that this parameter could be developed into a new and cost-effective clinical marker for inflammation and red blood cell deformation.

* Corresponding author.
E-mail addresses: alexis.darras@uni-saarland.de, alexis.charles.darras@gmail.com (A. Darras).

https://doi.org/10.1016/j.jcis.2024.10.039
Received 1 July 2024; Received in revised form 26 September 2024; Accepted 7 October 2024
Available online 10 October 2024

1. Introduction

The formation of a dried blood stain is a phenomenon that has garnered significant research interest, with applications ranging from low-cost diagnostic methods, e.g., for tuberculosis, thalassemia, and neonatal jaundice [1,2], to forensic investigations [3,4]. In the soft matter community, the evaporation of colloidal droplets resting on a substrate, i.e., a sessile droplet, has been an area of intensive research in recent decades, following the seminal work of Deegan et al. [5]. Various mechanisms have been highlighted as fundamentally important for the final structure of the deposits, with the coffee-ring effect being omnipresent. The coffee-ring effect refers to the fact that, for a small sessile droplet of a wetting liquid with a pinned contact line, an outward flow near the contact line typically drags the particles toward the pinned edge of the droplet due to the inhomogeneous evaporation rate along the droplet's surface [5]. However, when a sufficiently high salt concentration is considered, the dominant mechanism becomes solutal Marangoni recirculation due to the gradient of salt concentration. Indeed, a significant increase in salt concentration also leads to an increase in surface tension, and concentration gradients can therefore induce a substantial gradient in surface tension, which can create a central deposit of the particles [6–8].

In the case of blood evaporative deposits, the roles of temperature [9], ambient humidity [10], the substrate's nature, and the ions and proteins present in the plasma [11,12] on the final structure have been extensively studied. Moreover, seminal studies have shown the effects of red blood cell (RBC) properties by comparing rigidified cells or spheres with healthy RBCs [13], while others have highlighted the effect of dilution by studying patterns obtained from diluted whole blood in distilled water and Phosphate Buffered Saline (PBS), down to blood concentrations of around 10% [14]. However, the detailed influence of RBC properties, such as shape and aggregability, on the deposit growth and final state remains unclear. This is particularly relevant, as previous studies have demonstrated that, in the case of solid particles, the anisotropy of colloids can modify particle aggregation regimes, reverse the deposit pattern [15], and dictate their growth dynamics [16].

As RBCs aggregate into mostly linear structures called rouleaux in the presence of certain proteins [17–19], one can hypothesize that the length of these rouleaux acts as an effective particle eccentricity, influencing the structure of the evaporative deposit. The aggregability of RBCs, i.e., their tendency to form longer rouleaux and networks with wider gaps, is known to be heavily influenced by cell rigidity and fibrinogen concentration [18,20,21].

Thus, the main objective of this study is to determine whether evaporative deposits of dilute RBC suspensions show sensitivity to RBC aggregability and shape, which could be leveraged to develop low-cost screening methods for pathological changes in RBC aggregability and shape. We focus on droplets with volume fractions $\phi < 1\%$ of RBCs (compared to the physiological level of $\phi \approx 45\%$) in plasma- and PBS-based solutions. We observed a central deposit for the various suspending liquids with isotonic osmolarities. Building on this result, we created line-shaped droplets and studied how cell shape and aggregation modify the growth and final central linear deposit. We mixed plasma with serum to modify RBC aggregation [20], while varying the osmolarity of the PBS-based suspensions to alter RBC shape. All conditions led to growth consistent with the Kardar-Parisi-Zhang process in the presence of quenched disorder (KPZQ) [16,22]. However, the final sizes of the deposits varied as a function of cell shape, volume, and aggregability, indicating that studying these patterns could potentially serve as low-cost screening indicators for deformed RBCs or abnormal aggregation levels.

2. Methods

2.1. Ethics statement

Human blood withdrawal from healthy volunteers was performed after explicitly obtaining their informed consent. Blood withdrawal and handling were conducted in accordance with the Declaration of Helsinki and approved by the ethics committee "Aerztekammer des Saarlandes" (reference No. 176/21)

2.2. Experimental protocol

Fresh blood was drawn from healthy donors via venous blood sampling into tubes containing Ethylenediamine tetraacetic acid (EDTA) and a tube for serum (S-Monovette, Sarstedt, Nümbrecht, Germany). Cells were separated from the plasma by centrifuging the EDTA tubes for 7 minutes at 3000 rcf using a fixed-angle centrifuge (Hermle Z 36 HK, Hermle, Wehingen, Germany). The unit rcf stands for Relative Centrifugal Field, expressing the centrifugal acceleration as a multiple of gravitational acceleration g. Plasma was then obtained as the supernatant and was transferred immediately after centrifugation into a clean 1.5 mL Eppendorf tube using a micropipette. Serum was collected in a similar fashion, except that the blood was allowed to clot by leaving the collection tube undisturbed at room temperature for 30 minutes, according to the serum-tube manufacturer's guidelines (S-Monovette, Sarstedt, Nümbrecht, Germany). Clotted components were then removed by centrifuging with the same protocol as for the plasma. Serum was obtained as the supernatant. Afterwards, 1 mL samples with volume fraction $\phi = 3 \times 10^{-3}$ of RBCs were prepared by suspending the packed cells in PBS ($Gibco, USA$), plasma and/or serum. Samples were kept at room temperature for the duration of the experiments (less than 6 h).

In order to investigate whether changes in RBC shapes can lead to a different growth class of the edges obtained in the deposits, we also suspended RBCs in solutions of various osmolarities. In healthy individuals, RBCs at rest typically possess a biconcave disk shape. However, the osmolarity of the surrounding medium can change the shape of the RBCs according to the stomatocyte-discocyte-echinocyte (SDE) sequence [23–25]. To that end, solutions with osmolarities of $(130, 200, 300, 550, 800\,\text{mOsmol/L})$, with 5 mg/mL of fibrinogen to ensure aggregation between RBCs, were prepared according to the protocols described in the next paragraphs. Washed RBCs were then resuspended in each solution with the same volume fraction $\phi = 3 \times 10^{-3}$ as earlier. Representative shapes of RBCs as observed under the confocal microscope are shown in Fig. A.6.

To prepare the RBC suspensions with osmolarity lower than physiological and PBS values ($\approx 300\,\text{mOsmol/L}$), we first diluted fibrinogen from human plasma (Product code F3879-5G, 50-70% protein, ($\geq 80\%$ of protein is clottable) Sigma Aldrich, Burlington, Massachusetts, United States) in a solution of physiological osmolarity. For stability reasons, human plasma fibrinogen is typically stored as a powder containing around 60% protein by mass, stabilized with 15% sodium citrate and 25% NaCl. We experimentally determined that an iso-osmotic solution of fibrinogen in PBS can be reproduced by using 5% distilled water for each 1 mg/mL of fibrinogen (i.e., for each $1/0.6 \approx 1.67\,\text{mg/mL}$ of the powder). However, due to possible heterogeneity in the powder, the osmolarity of this solution was always checked with a freezing-point osmometer (Osmomat 3000basic, Gonotec, Berlin, Germany). Since this first step may require repetition to achieve the desired concentration of fibrinogen at the correct osmolarity, and because fibrinogen dissolves faster at 300 mOsmol/Lthan in solutions of lower osmolarity, we always first prepared an iso-osmotic solution with a fibrinogen concentration of $F_t * Osm_{iso}/Osm_t$. Here, $F_t = 5\,\text{mg/mL}$ is the target fibrinogen concentration, $Osm_{iso} = 300\,\text{mOsmol/L}$ is the osmolarity of the isotonic solution, and $Osm_t < Osm_{iso}$ is the target osmolarity. The isotonic solution was then diluted with distilled water, using proportions of Osm_t/Osm_{iso} of the isotonic fibrinogen solution and $1 - Osm_t/Osm_{iso}$ of distilled water. Finally, $45 \pm 5\,\text{mg/mL}$ of Bovine Serum Albumin (BSA) ($\geq 96\%$, Sigma Aldrich, Burlington, Massachusetts, United States) were added to the solution, both to prevent deformation of RBCs due to the glass effect and to limit salt crystallization at the end of the evaporation process. Red blood cells were then suspended in each solution following the previously described protocol.

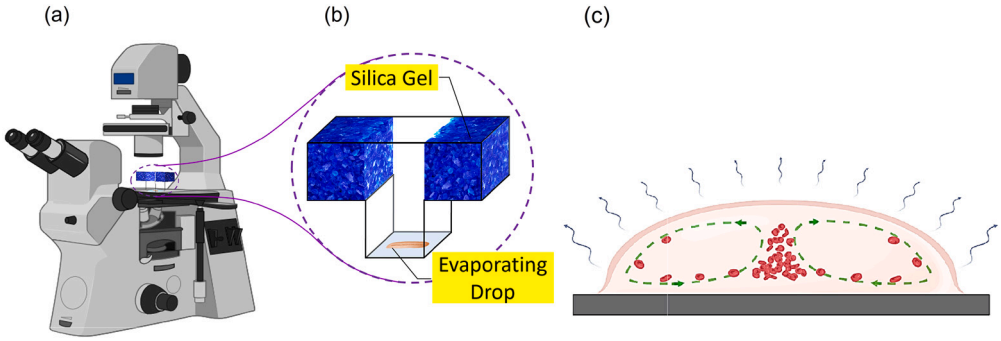

Fig. 1. Experimental setup: (a) Schematic of the inverted transmission microscope, and (b) the T-shaped drying chamber where the sample drop is placed on a microscopic slide. The slide's contact with the chamber is sealed with petroleum jelly. (c) Schematic of the solutal Marangoni flow inside the evaporating droplet, which transports the cells and gathers them in the center of the droplet. Such a flow pattern is observed in solutions with high salt concentration [6,26].

To prepare the RBC suspensions with osmolarity higher than physiological (and PBS) values (550, 800 mOsmol/L), isotonic solutions with 5 mg/mL of fibrinogen and 45 mg/mL of BSA were prepared as described previously. Afterwards, a mass $m = \Delta C\, V\, M/2$ of NaCl (>99.5, VWR, Radnor, Pennsylvania, USA) was added to the solution, where ΔC is the required increase in osmolarity, V is the volume of the solution, and $M = 58.44\,\mathrm{g/mol}$ is the molar mass of NaCl.

The final osmolarity of the solutions was always checked with a freezing-point osmometer and only used if the deviation was lower than 10% from the target value.

To create the deposits, a 5 μL pendant drop of the sample was formed at the tip of an adjustable 2-20 μL volume micropipette (Eppendorf, Hamburg, Germany). The pendant droplet was then placed on a glass slide (Microscope cover glass, ECN 631-1586, VWR, Radnor, Pennsylvania, USA), which had been previously cleaned with isopropanol and dried with compressed air (contact angle at rest of PBS was measured to be $52 \pm 3°$). To start an experiment with an elongated droplet, the 5 μL-drop was spread along 7 mm on the glass slide, using the same adjustable micropipette and a marked distance below the glass slide. To suppress the airflow and control the humidity of the environment in which the drop was placed for drying, a T-shaped hood was used. Both top sides of the hood were filled with completely dry blue silica gels to absorb humidity, as described in earlier works [7,8,27] (see Fig. 1). The glass slide with the droplet was placed under the microscope, and the T-shaped hood was adjusted on top of the glass slide with petroleum jelly (KORASILON-Paste, Kurt Obermeier GmbH, Bad Berleburg, Germany) on its base. The petroleum jelly ensured firm cohesion between the chamber and the glass slide and prevented the passage of airflow into the chamber. The drop was observed under an inverted transmission microscope (Nikon Eclipse $TE200$, Nikon, Tokyo, Japan) using a 4× objective. White light was sent through a short-pass filter with a cut-off wavelength of 450 nm (FESH0450, Thorlabs, Newton, New Jersey, USA). The filter was used to increase the contrast between the RBCs, whose absorption peak is at 415 nm due to hemoglobin, and the surrounding environment. Images of the evaporating drop were taken at intervals of 1 s using a CMOS camera (DMK 37BUX250, The Imaging Source, Charlotte, North Carolina, USA) attached to the microscope. Images were recorded until the droplet was completely dried and cracks appeared (see Appendix Fig. A.1), i.e., around 40 minutes. Examples of the obtained pictures are depicted in Fig. 2.

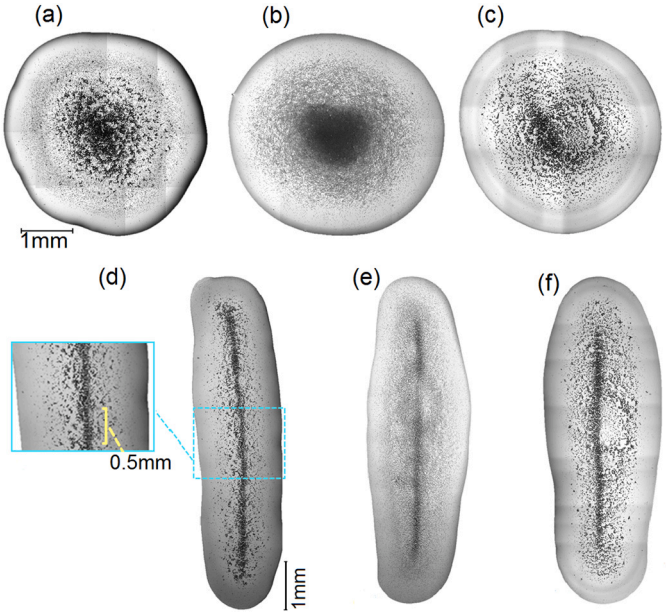

Fig. 2. Pictures of droplets from various suspensions of RBCs ($\phi = 3\,10^{-3}$), shortly before complete evaporation and the appearance of cracks (see Supp Fig. A.1 for completely dried deposits). (a-f) Whole drops were reconstructed by stitching series of pictures at higher zoom levels. (a-c) Spherical cap droplets of 5 μL; (d-f) Elongated droplets of 5 μL spread along 7 mm on the glass slide. (d) The inset shows the area of a single picture, where the deposition of red blood cells was investigated over time. Supernatants were (a and d) autologous plasma, (b and e) 4.5 mg/mL BSA solution in PBS, and (c and f) 5 mg/mL fibrinogen solution in PBS with 4.5 mg/mL BSA. The images were stitched together using ImageJ.

2.3. Image analysis

Using a homemade MATLAB code, the images of elongated droplets (see Fig. 2 (d-f)) were processed to binarize and isolate the central particle deposit. For each image, the code first averages the intensity perpendicularly to the main axis of the droplet, i.e., along y, and assesses the central position of the droplet as the y-coordinate with the minimal averaged intensity (since the RBCs have an absorption maximum at 420 nm, i.e., for blue light). The central deposit is then divided into two parts, splitting the picture at this central position, i.e., defining $y = 0$, as illustrated in Fig. 3(a). This effectively converts the central deposit into two growing edges. Analyzing both sides independently made it possible to monitor possible asymmetry in the droplet and/or deposit shape, which was used to reject data when significant differences were observed. The pictures were then binarized using an Otsu threshold on pixel intensity. Afterwards, only the connected components in contact with the central edge at $y = 0$ are considered as the growing edge, while other cells are discarded in further analysis. Furthermore, to ensure that only stable parts of the edge are considered, only pixels preserved in at least 9 out of 10 consecutive images are kept in the final picture. These final pictures, exemplified in Fig. 3(a), were analyzed to extract the properties of the deposit.

Deposits are characterized by their spatial extension, conventionally called profile height $h(x,t)$ measured as the distance between the center

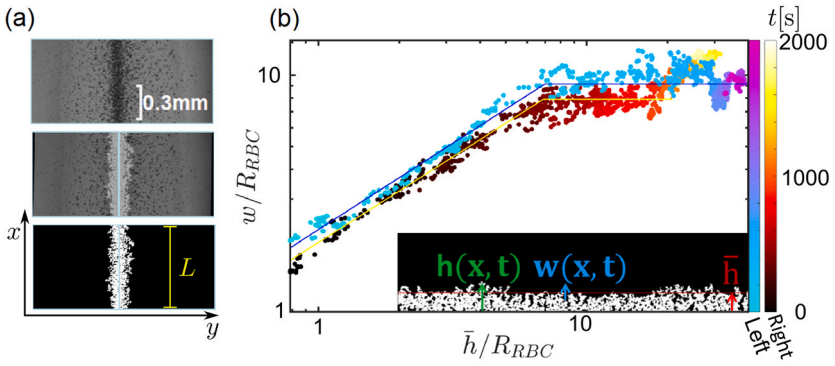

Fig. 3. Illustration of the image analysis process. (a) Snapshot of the central deposit with the raw experimental picture split at the detected center (for the resulting pattern of 0.3% volume suspension of RBCs in a 50-50 mixture of autologous serum and plasma), with overlaid final edges and the final binarized edges. This picture was taken 35 minutes after placing the drop on the slide. The x, y axes and the length of the system L are also indicated for further reference. (b) Scaling of the interface roughness width with average profile height for the superposition of the left side of the pattern and the right side of the pattern. Distances are normalized by the characteristic cell radius $R_{RBC} = 4.48\ \mu m$, in order to compare samples with possible radius changes (when various osmolarities are used). Solid lines are the fits used to obtain the parameter from Eq. (3). The slope of the first linear part, before saturation is reached, is the beta value. Color bars indicate the elapsed time based on the frame number after placing the drop on the surface of the microscope slide. (For interpretation of the colors in the figure(s), the reader is referred to the web version of this article.)

line and the farthest white pixel along y, at a given x (see Fig. 3(b)). The profile height is initially computed independently on the left and right sides of the center line. The growth of the central edge is then described through the relationship between $\bar{h}(t)$, the average of $h(x,t)$ along x, and $w(t)|_L$, the standard deviation of $h(x,t)$ evaluated on a system of size L along x, conventionally called the (roughness) width of the deposit (see Fig. 3(b) for graphical definitions).

2.4. Edge growth statistics

Usually, in order to describe the deposit growth quantitatively, both its mean profile height $\bar{h}(t)$ and roughness width $w(t)|_L$, which is the standard deviation of surface fluctuations around its mean value, are studied. For a discrete system, as our experimental pictures made of pixels, these two quantities are defined as [28,29]:

$$\bar{h}(t) = \frac{1}{L}\sum_{i=1}^{L} h(i,t) \tag{1}$$

where $h(i,t)$ indicates the profile height of the deposit at the i-th pixel along x at the time t, and L is the size of the system in pixels (see Fig. 3(a)). If the deposition rate (the number of particles reaching the surface per unit of time) is constant, the mean profile height increases linearly with time ($\bar{h} \sim t$). To quantify the growth process, the roughness width is investigated as a function of time

$$w(t)|_L = \sqrt{\frac{1}{L}\sum_{i=1}^{L}\left[h(i,t) - \bar{h}(t)\right]^2}\,. \tag{2}$$

For many phenomena [30–37], the roughness width w increases as a power of time

$$w(t)|_L \propto t^{\beta}\,, \tag{3}$$

where β is called the growth exponent and determines the time-dependent dynamics of the growth process. In experimental contexts, since defining the time zero is often difficult or arbitrary to some extent, a common approach consists in assuming that the scaling between w and t also translates between w and $\bar{h}$: $w(\bar{h})|_L \sim L^{\alpha} f(\frac{\bar{h}}{L^z})$. In our experiments, this beta coefficient was then obtained by fitting an piece-wise function, defined as an arbitrary straight line, continuously connected to a horizontal line (see Fig. 3(b)). The slope of the first line was considered to be the β parameter. The final horizontal line was used in the fit, because the roughness width eventually saturates at a value that increases as a power law of the system size:

$$w_{sat} \propto L^{\alpha} \tag{4}$$

The exponent α is the roughness exponent of the saturated surface. The above relations are often expressed in the relation introduced by Family–Vicsek [38]:

$$w(t)|_L \propto L^{\alpha} f\left(\frac{t}{L^z}\right), \tag{5}$$

where $z = \frac{\alpha}{\beta}$ is the dynamical exponent, and $f(u) \propto u^{\beta}$ if $u \ll 1$ and approaches a constant when $u \gg 1$ [29,38].

In order to measure the roughness coefficient α from Eq. (4), we calculate the local roughness width by dividing the pictures into windows of length l along the deposit axis, and average the results obtained from all the windows [39],

$$w^2(t)\Big|_l = \left\langle \frac{1}{l}\sum_{x=x_0}^{x_0+l}\left[h(x,t) - \bar{h}_l(t)\right]^2 \right\rangle_{x_0} \tag{6}$$

where $\bar{h}_l(t)$ is the average profile height of the selected window and <> indicates the ensemble averaging. According to Eq. (4), the local roughness width increases as a power law when the window size increases. Experimentally, it has already been shown that this exponent can follow various regimes, with transitions at given system sizes L [36]. The roughness exponent was then obtained by fitting the data obtained after $w(t)|_L$ saturated with a continuous piece-wise function, with two successive lines having positive slopes, followed by a constant value. The first line's slope was considered as the roughness exponent at short-length scales α_s. The slope of the second line is the roughness exponent at long length scales α_l (see Appendix Fig. A.2 for an example of the fitting process).

The previous scaling relationships can be used to define universality classes. In the context of evaporating droplets, it has been previously shown that the exponent β is sensitive to the shape of the particles, which can modify the growth regime of the edge formed by the coffee ring process. In particular, spheres have been shown to follow a Poisson process, characterized by $\beta = 0.5$ and $\alpha \approx 0$, while anisotropic particles, with anisotropic interactions, exhibited a growth belonging to the Kardar-Parisi-Zhang process with quenched disorder (KPZQ) with $\beta = 0.68$ and $\alpha = 0.63$ [16]. Given that the RBC shape can be altered by physio-chemical stresses or genetic diseases, one of the objectives of this work is to determine if the growth of the observed central edges can belong to various growth mechanisms. In particular, we tested if artificial changes in RBC shapes and aggregability can lead to a different growth class of the central Marangoni edge. To that end, we analyzed

the growth of the central edge obtained with various suspensions, using the image analysis described previously.

3. Results and discussion

In the beginning, dried deposits were obtained from spherical cap droplets with different suspending liquids (see Fig. 2(a-c)): autologous plasma, 4.5 mg/mL BSA solution in PBS, and in 1 mL of fibrinogen solutions (concentrations upto 5 mg/mL were used for fibrinogen in PBS, 4.5 mg/mL of BSA was also added in order to prevent the glass effect and the formation of slat crystals in the final dried deposits). As schematized in Fig. 1(c) and displayed in Fig. 2(a-c), RBCs migrate and accumulate towards the center of the drop due to a dominating solutal Marangoni flow. Hence, the pattern of all the dried drops in the conducted experiments includes central deposits of RBCs due to a solutal Marangoni recirculation loop. In order to study the growth of this central deposit, linear droplets were placed on a glass slide, as illustrated in Fig. 2(d-f). This setup allowed the use of classical 2D edge growth descriptions, previously used to model coffee rings [16] and described in Section 2.4. The dynamics of deposition were recorded at one frame per second with a 4X objective, around the middle of the droplet's line. A typical picture is displayed in the insert of Fig. 2(d). Interestingly, most of the droplet evaporation we observed occurred while the triple-phase line was pinned; the contact angle of the droplet decreased during the formation of the central edge, without influencing the exponents (α and β) describing the formation process of the central edge (see further results). It is therefore also likely that changing the initial contact angle without altering the liquid or the substrate (e.g., by using other deposition protocols that take advantage of the possible hysteresis observed in the formation of this contact angle) would only have a marginal influence on the parameters we measured.

As stated before, the main objective of this study is to determine whether evaporative deposits of dilute RBC suspensions present some sensitivity to RBC aggregability and shapes, which could be used to develop low-cost screening methods for pathological modifications. To determine whether the aggregability of the RBCs modifies the growth of the central deposit, we performed experiments by suspending 0.3% volume of RBCs in plasma, serum, and a 50-50 mixture of autologous serum and plasma.

Indeed, serum can basically be described as fibrinogen-free plasma, and fibrinogen is one of the main molecules promoting aggregation in blood samples. Using autologous serum offers a practical way to modify the RBCs' aggregability while maintaining other parameters as close as possible to their physiological conditions, as already employed in different studies [20,40,41]. The parameters obtained for three fibrinogen levels are displayed in Fig. 4, for fresh blood samples from 3 healthy donors and a repetition of 10 droplets. Although all suspensions demonstrated growth with an exponent close to that of a KPZQ process ($\beta \approx 0.68$ for KPZQ; our experimental values lie within $\beta \approx 0.64 \pm 0.04$), it is interesting to note that there is a significant difference in the distribution of the maximal roughness $w(t)|_L$ and maximal average profile height $\bar{h}(t)$ reached by the deposits over the course of the experiment. These maximal values are typically reached at the end of the experiment, but noise and minor perturbations (such as irregularities in the shape of the droplet) can slightly shift the observation time of these values. The significance of these variations is summarized by the range of p-values obtained from two-sample Kolmogorov-Smirnov tests. The p-values are the probabilities that the differences observed between the experimental measurements of two populations are due to random fluctuations from the same intrinsic continuous Probability Density Function. These tests have been performed using the function kstest2 in MATLAB. The ranges of p-values are abbreviated as ns (not significant) for $p > 0.1$, while the number n of stars $*$ refers to a significance level of $p < 10^{-n}$. Interestingly, changes in h_{max} and w_{max} seem to be more sensitive to an increase in fibrinogen levels, meaning that one could potentially detect inflammation with a method based on this observation, as fibrinogen is

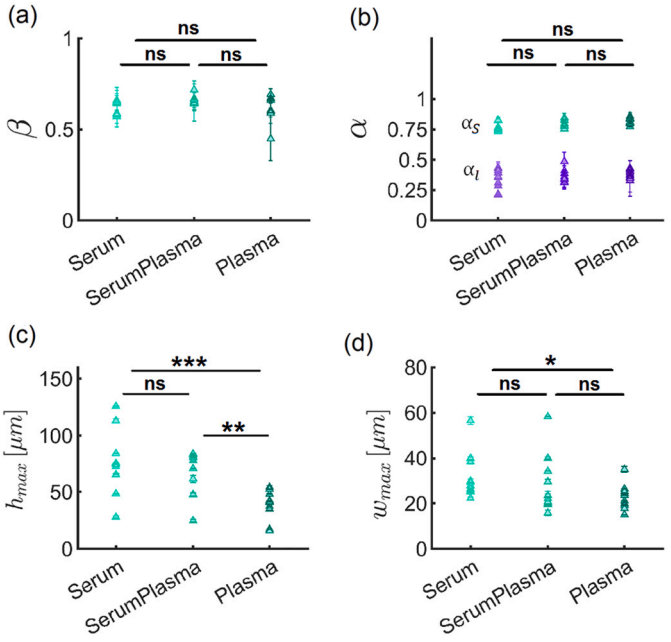

Fig. 4. Experimental results: (a) Average growth exponents, (b) Average roughness exponent, (c) Maximum profile height, and (d) Maximum roughness width, obtained for 0.3% red blood cell suspension formed in 1 mL of Serum, Plasma, and a 50-50 mixture of autologous serum and plasma (SerumPlasma). Measurements were repeated ten times for all three colloidal suspensions. The significance of the differences in the distributions is abbreviated as ns (not significant) for $p > 0.1$, while the number n of stars $*$ refers to a significance level of $p < 10^{-n}$.

a well-known inflammation marker [42]. Despite the fact that the internal convective movement is driven by Marangoni flow, there is no evidence that this systematic trend is due to a systematic change in the intensity of the solutal Marangoni flow, because there is no significant or systematic variation in the surface tension between serum, plasma, and the serum-plasma mixture (see Appendix Fig. A.3 for measurements with the pendant drop method). The most reasonable assumption is that the modification of the RBC aggregation is the parameter responsible for this change [18].

Since RBCs are one of the most deformable cell types, whose shape can be altered in pathologies, we also performed experiments to investigate whether artificial changes in RBC shapes and aggregation can lead to variations in the growth of the central Marangoni edge. More accurately, we tested if shapes from the Stomatocyte-Discocyte-Echinocyte (SDE) sequence, obtained via a change in osmolarity, would lead to any difference in the dynamics of the deposit formation. Although the osmolarity of the suspending phase should increase during evaporation of the droplet and possibly alter the shape of the RBCs during the experiments, we noticed that the significant part of the central deposit growth occurs within ten minutes of the evaporation process, while the overall evaporation process took around 40 minutes. The overall increase in osmolarity over the formation of the central deposit is therefore around $1/0.75 - 1$, i.e., an increase of approximately 33%, assuming a constant evaporation rate. This overall increase is too small to significantly alter the shape of the RBCs. Moreover, the osmolarity is probably inhomogeneous in the droplet, and the increase in osmolarity is likely limited to the edge of the droplet, since strong Marangoni recirculation is linked to a salt concentration gradient towards the edge of the droplet [26,43,44]. Finally, a closer inspection of the dried patterns shows that discocytes are still forming rouleaux in the case of an initial osmolarity of 300 mOsmol/L and that spherocytic or echinocytic shapes are still conserved in the dried deposit. Changes in RBC shapes during the formation of the deposit are therefore negligible.

Growth, roughness exponent, maximum profile height, and maximum roughness width obtained for various osmolarity levels are dis-

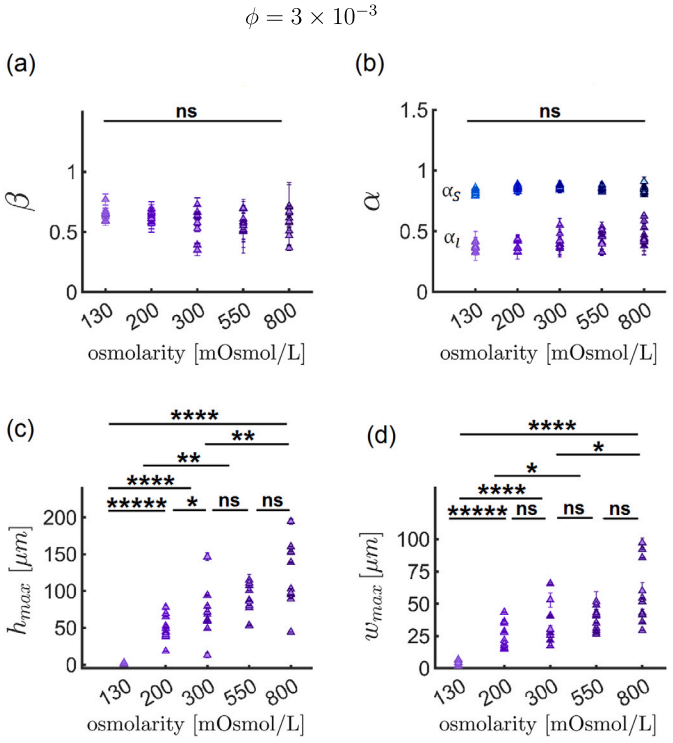

Fig. 5. Experimental results: (a) Average growth exponents, (b) Average roughness exponent, (c) Maximum profile height, and (d) Maximum roughness width, obtained for 0.3% red blood cell suspension were formed in 1 mL solutions of varying osmolarity. Measurements have been repeated ten times for all three colloidal suspensions. The abbreviation ns stands for not significant. The significance of p-values is defined as ns for $p > 0.1$, while the number n of stars $*$ refers to a significance level of $p < 10^{-n}$.

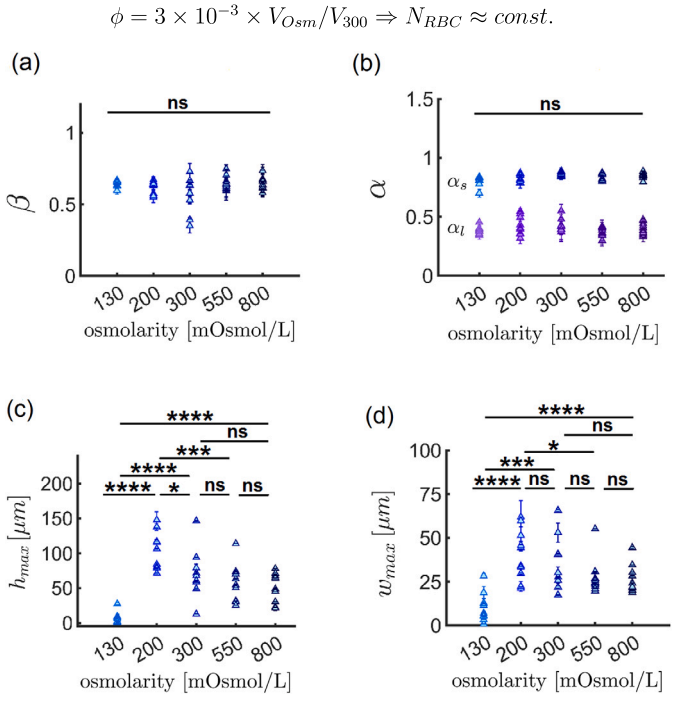

Fig. 6. Experimental results: (a) Average growth exponents, (b) Average roughness exponent, (c) Maximum profile height, and (d) Maximum roughness width, obtained for red blood cell suspensions with a volume fraction $\phi = 3 \times 10^{-3} \times V_{Osm}/V_{300}$, keeping the number of blood cells per milliliter constant. Measurements have been repeated ten times for all three colloidal suspensions. The abbreviation ns stands for not significant. The significance of p-values is defined as ns for $p > 0.1$, while the number n of stars $*$ refers to a significance level of $p < 10^{-n}$.

played in Fig. 5. According to previous results with inorganic particles, we expected some changes in the growth regime of the central deposit for various particle shapes, especially when moving from isotropic to anisotropic shapes [15,16]. The change in cell shape did not significantly impact the overall morphology or the universal class of growth. All samples were consistent with the KPZQ universality class, regardless of cell shape alterations. However, we also observed a significant increase in the maximal profile height of the central deposit, which was particularly sensitive to changes in osmolarity in the lower range, i.e., in the spherocyte-discocyte part of the SDE sequence. It is important to note that the volume of each blood cell also exhibits a clear dependence on osmolarity [45,46] (see Appendix Fig. A.4). Consequently, it was not clear at this stage whether this dependency is based on the shape of the erythrocytes or their volume in droplets of various initial osmolarities. However, we could rule out a change in the intensity of the Marangoni flow, as there was no significant difference in the surface tension of the various suspensions (see Appendix Fig. A.3).

As long as the volume fraction is kept below 1%, we noticed that increasing the volume fraction increases the maximum height and width but does not modify the formation dynamics. We therefore performed an additional set of experiments, maintaining a constant number of blood cells, instead of maintaining a constant volume fraction of $\phi = 3 \times 10^{-3}$ across all osmolarities. To that end, we estimated the average volume of RBCs at various osmolarities, V_{Osm}, through statistics from 3D scans performed with a confocal microscope (see Appendix Fig. A.4 for values), and suspended the RBCs with a volume fraction computed as $\phi = 3 \times 10^{-3} \times V_{Osm}/V_{300mOsmol/L}$, where $V_{300mOsmol/L} = 90\,\mu m^3$ is the standard volume of discocytes at a physiological osmolarity of 300 mOsmol/L (compatible with our measurements) [47]. With this change, we maintained a comparable number of RBCs in all samples, rather than a similar volume. Results with this protocol are depicted in Fig. 6. Interestingly, a significant increase in the maximal profile height is still observed from 130 mOsmol/L to 200 mOsmol/L, but the maximal roughness width decreases or remains constant at higher osmolarities. We can rule out that the osmolarity of the sample alone is responsible for the observed trend, as it is not reproduced when changing another parameter. Normalizing the dimensions of the central deposit by the length size of the cells (i.e., the cubic root of the average volume $V_{Osm}^{1/3}$ measured for a specific osmolarity) does not significantly alter the observed trends. Therefore, the volume of the cells alone does not explain the trends observed at low osmolarity in Figs. 6 and 5, although the trend observed in Fig. 6 at high osmolarity might be related to this change in volume, as correcting for the number of cells shows that there are no significant differences in the profile height of the deposit beyond 300 mOsmol/L in Fig. 5 (see Appendix, Fig. A.5 for the graph with normalization by the characteristic radius).

4. Conclusion

Our results showed that suspensions of red blood cells at low volume fractions ($\phi = 3 \times 10^{-3}$) form a central deposit, which contradicts the common assumption that blood evaporation is dominated by the classical coffee-ring effect [1–4,9–12,14,48]. These results suggest that Marangoni stresses should be incorporated into models used to explain the formation of cracks and patterns in dried blood deposits [48,49]. We demonstrated that the growth of this central deposit follows dynamics close to the predictions of the Kardar-Parisi-Zhang process with quenched disorder (KPZQ) scaling. This KPZQ scaling is robust enough to be observed in all osmolarities where the Spherocyte-Discocyte-Echinocyte transition can be seen, regardless of the shape adopted by the RBCs during the growth of the Marangoni edge. Our investigations also showed that the maximal profile height (in terms of average spatial extension of the 2D deposit) of this edge depends on

the properties of the red blood cells. In particular, higher aggregation of red blood cells results in a smaller deposit, while spherocytes tend to create smaller deposits, with the highest degree of significance. These results suggest that characterizing the size of this central deposit has potential applications as a clinical tool to detect changes in cell volume and/or geometry, which have not been considered before. However, our results also indicate that this size has a smaller sensitivity to changes corresponding to higher osmolarity levels. This suggests that developing automatic and highly reproducible elongated droplet shapes or exploring the effects of other control parameters, such as volume fraction, surrounding humidity, and temperature, might be an important step toward developing practical applications. Future work will focus on two aspects: (i) understanding the fundamental mechanisms of the transition between a central deposit and the accumulation of particles at the contact line as the volume fraction of cells increases, and (ii) quantifying how actual pathological modifications of RBC properties can be identified via patterns of blood evaporative deposits.

CRediT authorship contribution statement

Vahideh Sardari: Writing – review & editing, Writing – original draft, Visualization, Validation, Software, Methodology, Investigation, Formal analysis, Data curation, Conceptualization. **Mahsa Mohammadian:** Writing – review & editing, Investigation, Data curation. **Shima Asfia:** Writing – review & editing, Investigation, Data curation. **Felix Maurer:** Writing – review & editing, Software, Investigation, Formal analysis, Data curation. **Diana Örüm:** Writing – review & editing, Investigation, Data curation. **Ralf Seemann:** Writing – review & editing, Resources. **Thomas John:** Writing – review & editing, Software, Formal analysis. **Lars Kaestner:** Writing – review & editing, Resources, Methodology. **Christian Wagner:** Writing – review & editing, Resources, Funding acquisition. **Maniya Maleki:** Writing – review & editing, Formal analysis. **Alexis Darras:** Writing – review & editing, Writing – original draft, Supervision, Project administration, Methodology, Investigation, Funding acquisition, Formal analysis, Data curation, Conceptualization.

Declaration of competing interest

The authors declare that they have no known competing financial interests or personal relationships that could have appeared to influence the work reported in this paper.

Acknowledgements

V.S. acknowledges funding from a Visiting Research Scholar Grant of the Ministry of Science, Research and Technology of Iran for her research stay in Germany. A.D. acknowledges funding by the Young Investigator Grant of the Saarland University.

Appendix A. Supplementary material

Supplementary material related to this article can be found online at https://doi.org/10.1016/j.jcis.2024.10.039.

Data availability

Data will be made available on request.

References

[1] B.S. Sikarwar, M. Roy, P. Ranjan, A. Goyal, Automatic disease screening method using image processing for dried blood microfluidic drop stain pattern recognition, J. Med. Eng. Technol. 40 (5) (2016) 245–254.
[2] L. Bahmani, M. Neysari, M. Maleki, The study of drying and pattern formation of whole human blood drops and the effect of thalassaemia and neonatal jaundice on the patterns, Colloids Surf. A, Physicochem. Eng. Asp. 513 (2017) 66–75.
[3] Y. Liu, D. Attinger, K. De Brabanter, Automatic classification of bloodstain patterns caused by gunshot and blunt impact at various distances, J. Forensic Sci. 65 (3) (2020) 729–743.
[4] D. Attinger, K. De Brabanter, C. Champod, Using the likelihood ratio in bloodstain pattern analysis, J. Forensic Sci. 67 (1) (2022) 33–43.
[5] R.D. Deegan, O. Bakajin, T.F. Dupont, G. Huber, S.R. Nagel, T.A. Witten, Capillary flow as the cause of ring stains from dried liquid drops, Nature 389 (6653) (1997) 827–829.
[6] M. Rossi, A. Marin, C.J. Kähler, Interfacial flows in sessile evaporating droplets of mineral water, Phys. Rev. E 100 (3) (2019) 033103.
[7] A. Darras, N. Vandewalle, G. Lumay, Transitional bulk-solutal Marangoni instability in sessile drops, Phys. Rev. E 98 (6) (2018) 062609.
[8] A. Darras, N. Vandewalle, G. Lumay, Combined effects of Marangoni, sedimentation and coffee-ring flows on evaporative deposits of superparamagnetic colloids, Colloid Interface Sci. Commun. 32 (2019) 100198.
[9] A. Pal, A. Gope, G. Iannacchione, Temperature and concentration dependence of human whole blood and protein drying droplets, Biomolecules 11 (2) (2021) 231.
[10] W.B. Zeid, D. Brutin, Influence of relative humidity on spreading, pattern formation and adhesion of a drying drop of whole blood, Colloids Surf. A, Physicochem. Eng. Asp. 430 (2013) 1–7.
[11] R. Chen, L. Zhang, D. Zang, W. Shen, Blood drop patterns: formation and applications, Adv. Colloid Interface Sci. 231 (2016) 1–14.
[12] A. Pal, A. Gope, A. Sengupta, Drying of bio-colloidal sessile droplets: advances, applications, and perspectives, Adv. Colloid Interface Sci. 314 (2023) 102870.
[13] L. Lanotte, D. Laux, B. Charlot, M. Abkarian, Role of red cells and plasma composition on blood sessile droplet evaporation, Phys. Rev. E 96 (5) (2017) 053114.
[14] A. Pal, A. Gope, J.D. Obayemi, G.S. Iannacchione, Concentration-driven phase transition and self-assembly in drying droplets of diluting whole blood, Sci. Rep. 10 (1) (2020) 18908.
[15] P.J. Yunker, T. Still, M.A. Lohr, A. Yodh, Suppression of the coffee-ring effect by shape-dependent capillary interactions, Nature 476 (7360) (2011) 308–311.
[16] P.J. Yunker, M.A. Lohr, T. Still, A. Borodin, D.J. Durian, A.G. Yodh, Effects of particle shape on growth dynamics at edges of evaporating drops of colloidal suspensions, Phys. Rev. Lett. 110 (3) (2013) 035501.
[17] C. Wagner, P. Steffen, S. Svetina, Aggregation of red blood cells: from rouleaux to clot formation, C. R. Phys. 14 (6) (2013) 459–469.
[18] M. Brust, O. Aouane, M. Thiébaud, D. Flormann, C. Verdier, L. Kaestner, M. Laschke, H. Selmi, A. Benyoussef, T. Podgorski, et al., The plasma protein fibrinogen stabilizes clusters of red blood cells in microcapillary flows, Sci. Rep. 4 (1) (2014) 4348.
[19] P. Steffen, C. Verdier, C. Wagner, Quantification of depletion-induced adhesion of red blood cells, Phys. Rev. Lett. 110 (1) (2013) 018102.
[20] A.K. Dasanna, A. Darras, T. John, G. Gompper, L. Kaestner, C. Wagner, D.A. Fedosov, Erythrocyte sedimentation: effect of aggregation energy on gel structure during collapse, Phys. Rev. E 105 (2) (2022) 024610.
[21] A. Darras, K. Peikert, A. Rabe, F. Yaya, G. Simionato, T. John, A.K. Dasanna, S. Buvalyy, J. Geisel, A. Hermann, et al., Acanthocyte sedimentation rate as a diagnostic biomarker for neuroacanthocytosis syndromes: experimental evidence and physical justification, Cells 10 (4) (2021) 788.
[22] Z. Csahók, K. Honda, E. Somfai, M. Vicsek, T. Vicsek, Dynamics of surface roughening in disordered media, Phys. A, Stat. Mech. Appl. 200 (1–4) (1993) 136–154.
[23] G. Brecher, M. Bessis, Present status of spiculed red cells and their relationship to the discocyte-echinocyte transformation: a critical review, Blood 40 (3) (1972) 333–344.
[24] N.M. Geekiyanage, M.A. Balanant, E. Sauret, S. Saha, R. Flower, C.T. Lim, Y. Gu, A coarse-grained red blood cell membrane model to study stomatocyte-discocyte-echinocyte morphologies, PLoS ONE 14 (4) (2019) e0215447.
[25] G. Simionato, K. Hinkelmann, R. Chachanidze, P. Bianchi, E. Fermo, R. van Wijk, M. Leonetti, C. Wagner, L. Kaestner, S. Quint, Red blood cell phenotyping from 3d confocal images using artificial neural networks, PLoS Comput. Biol. 17 (5) (2021) e1008934.
[26] A. Marin, S. Karpitschka, D. Noguera-Marín, M.A. Cabrerizo-Vílchez, M. Rossi, C.J. Kähler, M.A. Rodríguez Valverde, Solutal Marangoni flow as the cause of ring stains from drying salty colloidal drops, Phys. Rev. Fluids 4 (4) (2019) 041601.
[27] A. Darras, F. Mignolet, N. Vandewalle, G. Lumay, Remote-controlled deposit of superparamagnetic colloidal droplets, Phys. Rev. E 98 (6) (2018) 062608.
[28] A.-L. Barabási, H.E. Stanley, Fractal Concepts in Surface Growth, Cambridge University Press, 1995.
[29] F. Family, Dynamic scaling and phase transitions in interface growth, Phys. A, Stat. Mech. Appl. 168 (1) (1990) 561–580.
[30] P. Meakin, R. Jullien, Restructuring effects in the rain model for random deposition, J. Phys. 48 (10) (1987) 1651–1662.
[31] Z. Csahók, T. Vicsek, Kinetic roughening in a model of sedimentation of granular materials, Phys. Rev. A 46 (8) (1992) 4577.
[32] M. Kurnaz, K. McCloud, J. Maher, Sedimentation of glass beads under the influence of gravity, Fractals 1 (04) (1993) 1008–1021.
[33] M. Kurnaz, J. Maher, Sedimentation to form rough, quasi-one-dimensional interfaces, Phys. Rev. E 53 (1) (1996) 978.
[34] T.J. Oliveira, F. Aarão Reis, Roughness exponents and grain shapes, Phys. Rev. E, Stat. Nonlinear Soft Matter Phys. 83 (4) (2011) 041608.
[35] K.V. McCloud, M.L. Kurnaz, J.V. Maher, Deposition-rate effects on rough surfaces formed by sedimenting particles, Phys. Rev. E 56 (5) (1997) 5768.

[36] K. McCloud, M. Kurnaz, The effect of the third dimension on rough surfaces formed by sedimenting particles in quasi-two-dimensions, Int. J. Mod. Phys. B 16 (08) (2002) 1217–1223.
[37] U. Cardak, K. McCloud, M. Kurnaz, Experimental and computational study of the effect of the system size on rough surfaces formed by sedimenting particles in quasi-two-dimensions, Granul. Matter 8 (2006) 81–86.
[38] F. Family, T. Vicsek, Scaling of the active zone in the eden process on percolation networks and the ballistic deposition model, J. Phys. A, Math. Gen. 18 (2) (1985) L75.
[39] V. Sardari, F. Safari, M. Maleki, Dynamics of the surface growth resulted from sedimentation of spheres in a Hele-Shaw cell containing a low-viscosity fluid, Phys. Fluids 36 (5) (2024) 053303, https://doi.org/10.1063/5.0200886.
[40] A. Darras, T. John, C. Wagner, L. Kaestner, Erythrocyte sedimentation rate: a physics-driven characterization in a medical context, J. Vis. Exp. 193 (2023) e64502.
[41] T. John, L. Kaestner, C. Wagner, A. Darras, Early stage of erythrocyte sedimentation rate test: fracture of a high-volume-fraction gel, PNAS Nexus 3 (1) (2024) pgad416.
[42] D.R. Germolec, K.A. Shipkowski, R.P. Frawley, E. Evans, Markers of inflammation, in: Immunotoxicity Testing: Methods and Protocols, 2018, pp. 57–79.
[43] N. Shahidzadeh-Bonn, S. Rafaı, D. Bonn, G. Wegdam, Salt crystallization during evaporation: impact of interfacial properties, Langmuir 24 (16) (2008) 8599–8605.
[44] N. Shahidzadeh, M.F. Schut, J. Desarnaud, M. Prat, D. Bonn, Salt stains from evaporating droplets, Sci. Rep. 5 (1) (2015) 10335.
[45] M. Friebel, J. Helfmann, M.C. Meinke, Influence of osmolarity on the optical properties of human erythrocytes, J. Biomed. Opt. 15 (5) (2010) 055005.
[46] P. Heubusch, C.Y. Jung, F.A. Green, The osmotic response of human erythrocytes and the membrane cytoskeleton, J. Cell. Physiol. 122 (2) (1985) 266–272.
[47] C. Brugnara, D.C. Tosteson, Cell volume, k transport, and cell density in human erythrocytes, Am. J. Physiol., Cell Physiol. 252 (3) (1987) C269–C276.
[48] D. Roy, K.K. Dewangan, A. Rasheed, S. Jain, A. Singh, D. Chakravortty, S. Basu, et al., Insights into the mechanics of sessile whole blood droplet evaporation, arXiv preprint, arXiv:2402.12334, 2024.
[49] M.G. Hennessy, R.V. Craster, O.K. Matar, Drying-induced stresses in poroelastic drops on rigid substrates, Phys. Rev. E 105 (5) (2022) 054602.